

# Compressive Response of Lightweight Ceramic Ablators: Silicone Impregnated Reusable Ceramic Ablator

Kelly E. Parmenter,\* Karl Shuman,<sup>†</sup> and Frederick Milstein<sup>‡</sup>  
*University of California, Santa Barbara, Santa Barbara, California 93106*

and

Christine E. Szalai,<sup>§</sup> Huy K. Tran,<sup>||</sup> and Daniel J. Rasky\*\*  
*NASA Ames Research Center, Moffett Field, California 94035-1000*

Silicone impregnated reusable ceramic ablaters are highly porous fibrous ceramic substrates that are partially impregnated with silicone. The ablaters are used as heat shields for planetary entry. The compressive responses of virgin and charred ablaters, and their corresponding fibrous substrates, are reported. The fibers in the materials tend to be randomly and uniformly aligned parallel to a preferred plane, resulting in anisotropic mechanical properties. Compressive loads, applied either parallel or normal to the preferred fiber-alignment plane, yielded initial stress-strain responses that were fairly linear, to strains of about 1 or 2%. For virgin ablaters loaded normal to the fiber-alignment plane, the initial linear response was followed by a rapid decrease in the slope of the stress-strain curve, after which the stress increased asymptotically with strain, to strains over 80%, and stresses approaching 10 MPa, without macroscopic failure. In all other cases, after the initial linear response, the stress varied in an erratic, roughly horizontal, manner, without exceeding about 3 MPa. This erratic stress path indicates discontinuous breaking of the bonds between the fibers and/or buckling of the fibers. Good correlation between compressive strength and hardness was found among materials with this latter response. Comparisons are made with the behavior of phenolic impregnated carbon ablator.

## Nomenclature

|                      |   |   |
|----------------------|---|---|
| $A$                  | = | indentation surface area, $\pi D\delta$ , mm <sup>2</sup>                         |
| $D$                  | = | diameter of hardness indenter, mm   |
| $e$                  | = | energy density [defined in Eq. (3)], MJ/m <sup>3</sup>                            |
| $E_i$                | = | initial Young's modulus, MPa  |
| $E_j$                | = | secant modulus, $j = 1, 2$ [defined in Eq. (1)], MPa                              |
| $H$                  | = | $L_{\max}/A$ , hardness, MPa  |
| $L_{\max}$           | = | maximum load during hardness test, N  |
| $S$                  | = | compressive strength, MPa   |
| $S_0$                | = | stress at initial fracture, MPa   |
| $\delta$             | = | depth of penetration of hardness indenter, mm                                     |
| $\epsilon$           | = | strain, mm/mm   |
| $\epsilon_c$         | = | critical strain [numerical parameter in Eq. (2), values listed in Table 2], mm/mm |
| $\epsilon_j$         | = | strain at stress $\sigma_j$ , $j = 1, 2$ , mm/mm                                  |
| $\epsilon_S$         | = | strain at $S$ , mm/mm   |
| $\epsilon_0$         | = | strain at initial fracture, mm/mm   |
| $\sigma$             | = | stress, MPa   |
| $\sigma_a, \sigma_b$ | = | numerical parameter in Eq. (2) [values listed in Table 2], MPa                    |
| $\sigma_j$           | = | stress values, $j = 1, 2$ , used to calculate $E_j$ in Eq. (1), MPa               |

|            |   |   |
|------------|---|---|
| $\sigma_Y$ | = | yield stress, MPa   |
| $\sigma_1$ | = | $0.5S$ , MPa  |
| $\sigma_2$ | = | $0.9S$ (if $0.9S \leq S_0 \leq S$ ) or equal to $S_0$ (if $S_0 < 0.9S$ ), MPa |

## Introduction

THIS paper is the second in a series of papers that present results of experimental studies of the mechanical behavior of lightweight ceramic ablator (LCA) materials. The impetus for (and importance of) these studies is discussed in the Introduction to our initial paper.<sup>1</sup> Briefly, LCAs were developed at the Thermal Protection Materials and Systems Branch at NASA Ames Research Center for use as heat shields on planetary entry vehicles. LCAs are highly porous fibrous ceramic substrates that are partially impregnated with organic resins.<sup>2</sup> The principal types of LCAs are silicone impregnated reusable ceramic ablator (SIRCA) and phenolic impregnated carbon ablator (PICA). SIRCA is used in applications where the heat fluxes are 200 W/cm<sup>2</sup> or less, and PICA is used for heat fluxes greater than 400 W/cm<sup>2</sup>. SIRCA was the heat shield on the aft plate of Mars Pathfinder and was chosen for the leading edges and nose cap of the X-34 vehicle.<sup>3</sup> SIRCA has also been adopted for use on the back interface plates of the entry aeroshells of both Mars Exploration Rovers, scheduled for launch in 2003, and recently Kistler Corporation has adopted SIRCA for the nose cap and other high heating areas on their proposed K-1 reusable launch vehicle. PICA was chosen as the heat shield for Stardust Sample Return Capsule's forebody<sup>4</sup> and is a candidate for future outer planet missions (to Jupiter, Saturn, Neptune, and their moons) that are anticipated toward the end of the current decade.

The thermal performance and ablation characteristics of LCAs have been studied extensively by Tran,<sup>2</sup> Tran et al.,<sup>4–7</sup> and Chen and Milos.<sup>8</sup> Although most experimental work on LCAs to date has been on thermal properties, Milos and Squire<sup>3</sup> conducted thermostructural analyses that included the results of three-point and cantilever bending tests on SIRCA. More recently, Marschall and Cox<sup>9</sup> and Marschall and Milos<sup>10</sup> measured the gas permeability of SIRCA, PICA, and several rigid fibrous refractory substrates.

Previously, the compressive and hardness responses of PICA, charred PICA, and PICA's carbon fiber substrate, Fiberform<sup>®</sup>, were presented.<sup>1</sup> In the present paper, results are presented from compression and hardness tests on two types of SIRCA, in both

Received 26 February 2001; revision received 24 September 2001; accepted for publication 2 October 2001. Copyright © 2002 by the American Institute of Aeronautics and Astronautics, Inc. All rights reserved. Copies of this paper may be made for personal or internal use, on condition that the copier pay the \$10.00 per-copy fee to the Copyright Clearance Center, Inc., 222 Rosewood Drive, Danvers, MA 01923; include the code 0022-4650/02 \$10.00 in correspondence with the CCC.

\*Research Associate, Departments of Mechanical Engineering and Materials; kellyp@west.net.

<sup>†</sup>Research Assistant, Departments of Mechanical Engineering and Materials; ceiluer@engineering.ucsb.edu.

<sup>‡</sup>Professor, Departments of Mechanical Engineering and Materials; frdmilstn@engineering.ucsb.edu.

<sup>§</sup>Research Scientist, Thermal Protection Materials and Systems Branch; cszalai@mail.arc.nasa.gov. Senior Member AIAA.

<sup>||</sup>Research Scientist, Thermal Protection Materials and Systems Branch; htran@mail.arc.nasa.gov. Member AIAA.

\*\*Senior Scientist, Space Technology Division; drasky@mail.arc.nasa.gov. Senior Member AIAA.

their virgin and charred states, and on their corresponding fibrous substrates. The materials were tested with uniaxial loads parallel to, and transverse to, the plane of preferred fiber alignment, to determine the anisotropy of the mechanical response. In addition, the prominent characteristics of PICA and SIRCA under compressive loading are compared.

In the following two sections of this paper, the samples that were tested and the compression and hardness test procedures that were used are described. Then, a discussion of the compression and hardness results for each material and loading condition is presented.

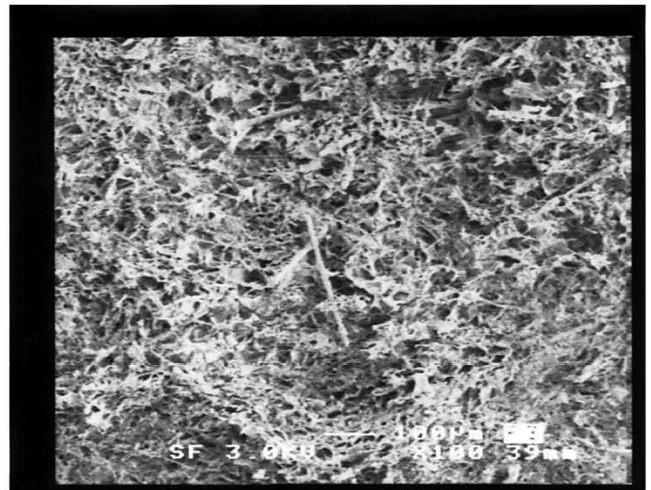
## Materials and Test Procedures


### Materials

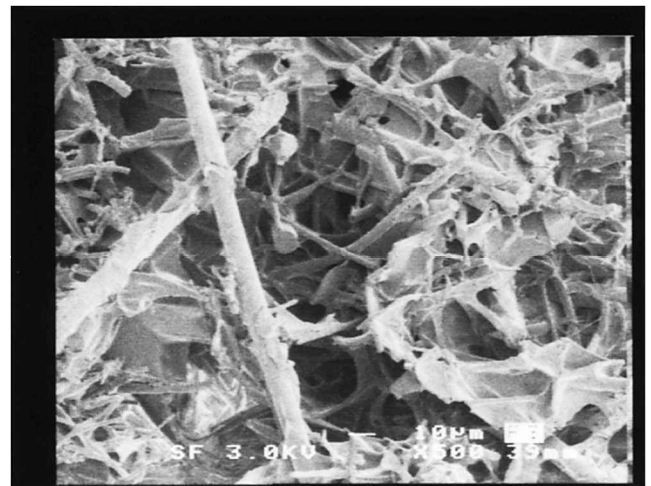
Compression and hardness measurements were made on two types of SIRCA, with NASA designations 15A and 15F, wherein the 15 indicates the approximate density in pounds mass per cubic foot, and A and F refer to the type of substrate. In particular, A signifies Ames insulation material (AIM), which is made from silica fibers ( $\sim 3\text{-}\mu\text{m}$  diam), and F designates a fibrous refractory composite insulation (FRCI), which consists of 78% silica fibers ( $\sim 3\text{-}\mu\text{m}$  diam), 20% Nextel 312 fibers ( $\sim 8\text{-}\mu\text{m}$  diam), and 2% SiC powder (1200 grit). Nextel 312 consists of 62.6%  $\text{Al}_2\text{O}_3$ , 24.4%  $\text{SiO}_2$ , and 12.9%  $\text{B}_2\text{O}_3$ . Both types of SIRCA are impregnated with silicone resin. The average density of the SIRCA specimens tested in the present study ranged from about 245 to 330  $\text{kg/m}^3$  for SIRCA 15A, and from 240 to 260  $\text{kg/m}^3$  for SIRCA 15F. The average density of the substrate materials that were tested ranged from about 165 to 190  $\text{kg/m}^3$  for AIM and from 170 to 220  $\text{kg/m}^3$  for FRCI. Density is taken to be the mass of a sample divided by its bulk volume as determined by its exterior dimensions; average density is the mean average, taken over individual density measurements on different samples. Numerical values of density with  $\pm$  values are average values with standard deviations.


In earlier work,<sup>2,5-7</sup> conditions encountered during atmospheric entry were simulated in the 60 MW Interaction Heating Facility and 20 MW Aerodynamic Heating Facility at NASA Ames Research Center. The LCAs were found to ablate and develop a char layer (on the order of a few millimeters thick) with material properties that vary with surface depth. Thus, the influence of charring on the mechanical properties of the LCAs is also of interest. To obtain uniformly charred SIRCA for mechanical testing in the present study, specimens were pyrolyzed in a tube furnace, in an argon atmosphere, at 1000°C for 10 min, and then the furnace was turned off and the specimens were cooled to room temperature. The cooling rate was approximately 50°C/min in the beginning, and then decreased gradually to about 20°C/min toward the end. This process caused decomposition of the silicone resin and yielded fibrous substrates coated in char residue. The average postcharred density of SIRCA ranged from about 240 to 270  $\text{kg/m}^3$  for SIRCA 15A and from about 240 to 300  $\text{kg/m}^3$  for SIRCA 15F.

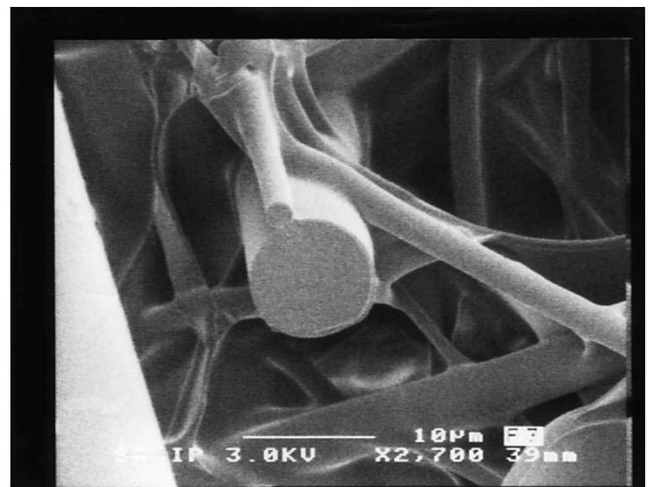
As in the case of PICA, the fibers in the substrates of SIRCA tend to be randomly and uniformly aligned parallel to a preferred plane, resulting in highly anisotropic mechanical properties that are dependent on the orientation of the plane of preferred fiber alignment with respect to the direction of loading during measurement. For brevity, the plane of preferred fiber alignment is called simply the preferred plane, and, in discussions of the hardness and compression data, the terms transverse loading or transverse compression refer to loads applied perpendicular to the preferred plane, whereas parallel loading or parallel compression designate loads parallel to the preferred plane. It is mentioned, in passing, that a study of fracture surfaces, produced in various modes of loading (including tension, shear, and bending, as well as compression), has been undertaken via scanning electron microscopy. Comprehensive results of this study will be available in due course. Here, to illustrate general microstructural features, photomicrographs of fracture surfaces of virgin SIRCA and charred SIRCA are shown, at various levels of magnification, in Figs. 1 and 2, respectively. Specifically, Fig. 1 shows a fracture surface at three levels of magnification of a SIRCA 15F specimen that was tested in transverse compression. The views are oblique relative to the preferred plane of fiber alignment. A relatively high degree of porosity is evident in the photomicrographs

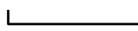


a) 200  $\mu\text{m}$ : 

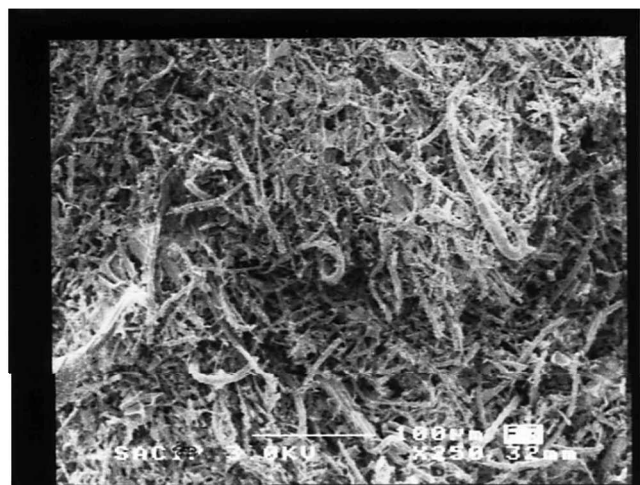



b) 40  $\mu\text{m}$ : 




c) 10  $\mu\text{m}$ : 

**Fig. 1** Scanning electron photomicrographs, at three levels of magnification, of a fracture surface of a SIRCA 15F specimen that was fractured in transverse compression.



a) 100  $\mu\text{m}$ : 



b) 5  $\mu\text{m}$ : 

**Fig. 2** Scanning electron photomicrographs, at two levels of magnification, of a region of a charred SIRCA 15A surface that was fractured in parallel compression.

of SIRCA 15F. Figure 2 shows, under two levels of magnification, a region of a fracture surface of a charred SIRCA 15A specimen that was tested in parallel compression. The planes of the images in Fig. 2 are roughly coincident with the preferred plane of fiber alignment.

#### Test Procedures

Compression and hardness tests, under both parallel and transverse loads, were carried out with the same procedures described previously by the present authors.<sup>1</sup> Loads were applied to the specimens in a displacement-controlled Instron 1123 test machine. Loads were measured with a precision load cell that is National Institute of Standards and Testing traceable and calibrated to 1% of full scale. In addition, calibrations of the load cell by the dead weight method, at low loads (between 5 and 30 N), were found to be within 2% throughout the range of loads that were tested. Compression test specimens had nominal dimensions of  $12.7 \times 12.7 \times 25.4$  mm. The load was applied parallel to the long axis of the specimens. One portion of the compression test fixture consisted of a self-aligning "frictionless" hemisphere. The crosshead speed ranged from 0.102 mm/min (for parallel loading) to 0.762 mm/min (for transverse loading). Measured values of load and displacement were converted to values of stress and strain, respectively, by dividing the

loads by the corresponding initial cross-sectional areas of the specimens and the displacements by the corresponding initial lengths of the specimens.

Hardness indents were made with a steel ball of diameter  $D = 19.05$  mm. A preload of 1 N was applied to minimize surface effects. The load was then increased to a maximum value  $L_{\max}$  (usually about 30 N) and subsequently reduced to the preload value, where the depth of penetration  $\delta$  was determined. Hardness  $H$  is defined by the relation  $H = L_{\max}/A$ , where the indent surface area  $A$  is approximated by the relation  $A = \pi D\delta$ . In the hardness measurements, the displacement was measured with a linear variable differential transformer, with a range of  $\pm 6.35$  mm and a resolution of 3  $\mu\text{m}$ . The crosshead speed was 0.102 mm/min. This procedure was developed by Parmenter and Milstein<sup>11</sup> to measure the hardness of fiber reinforced silica aerogels.

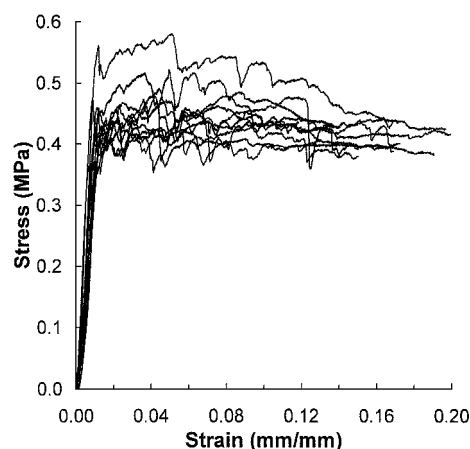
Exploratory tests were carried out to determine suitable values of  $L_{\max}$  for use in hardness testing. Generally, the LCAs and their respective substrates responded well to maximum loads of 30 N; however, SIRCA 15F began to crack in some cases at loads greater than 20 N, resulting in choppy load-displacement curves. To verify that this behavior did not unduly influence the test results, half of the indents on SIRCA 15F were made with nominal  $L_{\max}$  values of 20 N and the other half with nominal  $L_{\max}$  values of 30 N. No appreciable load dependence was observed for the hardness of SIRCA 15F between about 20 and 30 N. However, there was a tendency for the apparent measured hardness of SIRCA 15F to decrease at loads higher than 30 N because of cracking and surface cave-in, particularly when the load on the indenter was parallel to the plane of preferred fiber alignment. All other hardness measurements reported herein (and in Ref. 1) were made with nominal  $L_{\max}$  values of 30 N.

## Results and Discussion

### Compressive Response

Two distinct types of compressive stress-strain responses were observed among the specimens tested for the present work and for Ref. 1. For brevity, these are referred to as type 1 behavior and type 2 behavior. Type 1 behavior was exhibited in all parallel compression tests and in the transverse tests of AIM, FRCI, charred SIRCA 15A, and charred SIRCA 15F. Type 2 behavior was found in the transverse compression tests of all virgin LCAs (i.e., PICA, SIRCA 15A, and SIRCA 15F), Fiberform, and charred PICA. The type 1 and 2 behaviors are described in the following paragraphs.

Although our main interest is in the behavior of the composite LCA materials, it is nevertheless instructive to begin by examining the compressive behavior of the bare substrates. Figures 3 and 4, respectively, each show the stress-strain responses of about a dozen AIM and FRCI specimens that were loaded in parallel compression. Figures 5 and 6 show the analogous behaviors for transverse loading over the same range of strain, that is, from 0 to 0.2 mm/mm. The stress-strain response of each substrate is qualitatively the same, regardless of orientation. Such qualitative behavior is characterized

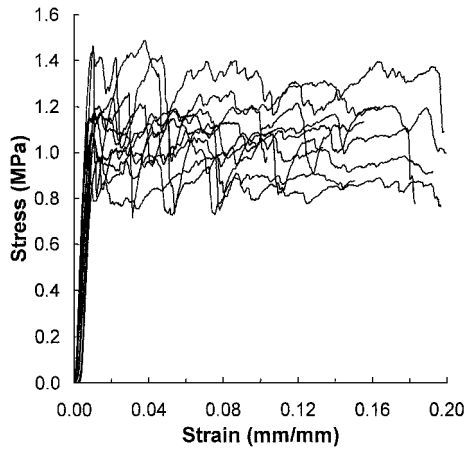
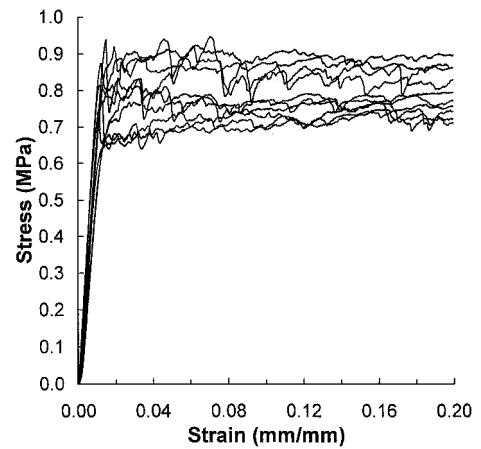
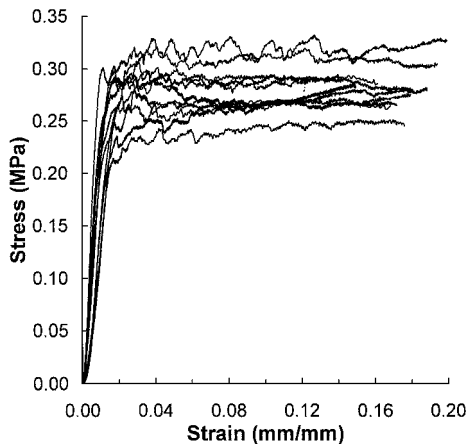


**Fig. 3** Stress-strain curves obtained from parallel-compression testing of AIM; density =  $192 \pm 8$  kg/m<sup>3</sup>.

**Table 1** Mechanical properties of SIRCA, charred SIRCA, and the fibrous substrates AIM and FRCI under compressive loading, derived from Figs. 3–8 and 10–13; Fiberform, PICA, and charred PICA (from Ref. 1) included for comparison<sup>a</sup>

| Row | Material             | Mode of loading | No. of samples | Density, kg/m <sup>3</sup> | $S_0$ , MPa     | $\epsilon_0$ , mm/mm | $S$ , MPa   | $\epsilon_S$ , mm/mm | $E_1$ , MPa | $E_2$ , MPa |
|-----|----------------------|-----------------|----------------|----------------------------|-----------------|----------------------|-------------|----------------------|-------------|-------------|
| 1   | AIM                  | P <sup>b</sup>  | 12             | 192 ± 8                    | 0.43 ± 0.05     | 0.010 ± 0.002        | 0.47 ± 0.04 | 0.054 ± 0.030        | 46 ± 9      | 43 ± 11     |
| 2   | FRCI                 | P               | 11             | 172 ± 5                    | 1.16 ± 0.17     | 0.009 ± 0.002        | 1.21 ± 0.15 | 0.057 ± 0.047        | 148 ± 22    | 135 ± 24    |
| 3   | AIM                  | T <sup>c</sup>  | 11             | 165 ± 2                    | 0.27 ± 0.03     | 0.015 ± 0.003        | 0.29 ± 0.02 | 0.091 ± 0.059        | 26 ± 6      | 18 ± 4      |
| 4   | FRCI                 | T               | 10             | 182 ± 8                    | 0.78 ± 0.09     | 0.013 ± 0.003        | 0.84 ± 0.07 | 0.081 ± 0.068        | 72 ± 9      | 62 ± 15     |
| 5   | S15A <sup>d</sup>    | P               | 12             | 311 ± 9                    | 1.38 ± 0.09     | 0.022 ± 0.002        | 1.38 ± 0.09 | 0.022 ± 0.002        | 80 ± 8      | 71 ± 4      |
| 6   | S15F <sup>e</sup>    | P               | 8              | 260 ± 4                    | 2.08 ± 0.12     | 0.017 ± 0.001        | 2.08 ± 0.12 | 0.017 ± 0.001        | 130 ± 5     | 126 ± 5     |
| 7   | Ch <sup>f</sup> S15A | P               | 13             | 243 ± 8                    | 1.41 ± 0.42     | 0.020 ± 0.008        | 1.51 ± 0.32 | 0.028 ± 0.009        | 88 ± 14     | 78 ± 23     |
| 8   | Ch S15F              | P               | 12             | 253 ± 21                   | 2.38 ± 0.33     | 0.018 ± 0.003        | 2.40 ± 0.32 | 0.026 ± 0.017        | 138 ± 17    | 141 ± 23    |
| 9   | Ch S15A              | T               | 12             | 268 ± 12                   | 1.19 ± 0.58     | 0.019 ± 0.006        | 1.22 ± 0.57 | 0.038 ± 0.030        | 70 ± 19     | 70 ± 28     |
| 10  | Ch S15F              | T               | 12             | 244 ± 16                   | 1.71 ± 0.91     | 0.022 ± 0.007        | 1.80 ± 0.85 | 0.124 ± 0.107        | 89 ± 46     | 85 ± 47     |
| 11  | Fiberform            | P               | 10             | 187 ± 6                    | NA <sup>g</sup> | NA                   | 0.81 ± 0.08 | 0.041 ± 0.011        | 57 ± 12     | 32 ± 3      |
| 12  | PICA                 | P               | 18             | 220 ± 4                    | 1.54 ± 0.09     | 0.017 ± 0.002        | 1.55 ± 0.09 | 0.023 ± 0.011        | 143 ± 17    | 106 ± 9     |
| 13  | Ch PICA              | P               | 11             | 225 ± 8                    | NA              | NA                   | 1.79 ± 0.43 | 0.031 ± 0.006        | 107 ± 19    | 78 ± 21     |

<sup>a</sup>Numerical values following the ± signs are standard deviations. <sup>b</sup>Parallel. <sup>c</sup>Transverse. <sup>d</sup>SIRCA 15A. <sup>e</sup>SIRCA 15F. <sup>f</sup>Charred. <sup>g</sup>NA, not available.

**Fig. 4** Stress-strain curves obtained from parallel-compression testing of FRCI; density = 172 ± 5 kg/m<sup>3</sup>.**Fig. 6** Stress-strain curves obtained from transverse-compression testing of FRCI; density = 182 ± 8 kg/m<sup>3</sup>.**Fig. 5** Stress-strain curves obtained from transverse-compression testing of AIM; density = 165 ± 2 kg/m<sup>3</sup>.

herein as type 1. In Figs. 3–6, initially, the stress increases rather linearly with strain, up to strains of about 1% (0.01 mm/mm). Then, following initial fracture, the stress varies with strain on an erratic horizontal path that is indicative of continuing internal fracturing. During this stage, bonds between fibers, and/or the fibers themselves, apparently are breaking. Table 1 lists mechanical properties derived from Figs. 3–6. The entries in Table 1 include the stress  $S_0$  and strain  $\epsilon_0$  at initial fracture, the compressive strength  $S$  (i.e., the maximum stress), the strain  $\epsilon_S$  at which the maximum stress occurs, and two secant moduli  $E_1$  and  $E_2$ . The determinations of  $\epsilon_0$ ,  $\epsilon_S$ , and the secant moduli are reckoned to reference states at which the

stress is 0.05 MPa to eliminate initial transient effects. The secant moduli, which are a measure of stiffness, are the slopes defined by

$$E_j = \frac{[\sigma_j - 0.05 \text{ MPa}]}{[\epsilon_j - \text{strain at } 0.05 \text{ MPa}]} \quad (1)$$

where, for each sample,  $\epsilon_j$  = strain at  $\sigma_j$ ,  $\sigma_1 = 0.5S$ , and  $\sigma_2 = 0.9S$ . (Or, if a definitive initial fracture occurred at  $S_0 < 0.9S$ , then  $\sigma_2 = S_0$ , so that all  $\epsilon_j \leq \epsilon_0$ .) Although a strongly anisotropic response is not evident in the qualitative behavior of the bare substrates, there is definite quantitative anisotropy, as is readily seen from rows 1–4 of Table 1. Each substrate material is stronger and stiffer in parallel loading, and FRCI is stronger and stiffer than AIM. Specifically, for each substrate, in parallel loading, both  $S_0$  and  $S$  are about 50% greater, and the secant moduli are about 100% greater, than in transverse loading. In each mode of loading, the values of  $S_0$  and  $S$  and the secant moduli of FRCI are about three times the corresponding values for AIM.

Figures 7 and 8, respectively, show the stress-strain responses of specimens of SIRCA 15A and SIRCA 15F that were loaded in parallel compression. The parallel loading responses of the SIRCA materials exhibit the type 1 behavior that is characteristic of the substrates, as seen in Figs. 7 and 8 and in rows 5 and 6 of Table 1. Figures 7 and 8 employ a smaller range of strain than Figs. 3–6, to display clearly the initial, relatively linear, response and initial fracture. Figure 9 displays representative parallel compressive responses of both types of SIRCA and PICA over a larger range of strain. The compressive strengths of these samples are 1.45, 2.15, and 1.50 MPa, respectively, for SIRCA 15A, SIRCA 15F, and PICA. At large strains, PICA undergoes macroscopic fracture and crumbling, and the stress tends toward zero; however, both types of SIRCA continue to exhibit the erratic, roughly horizontal,

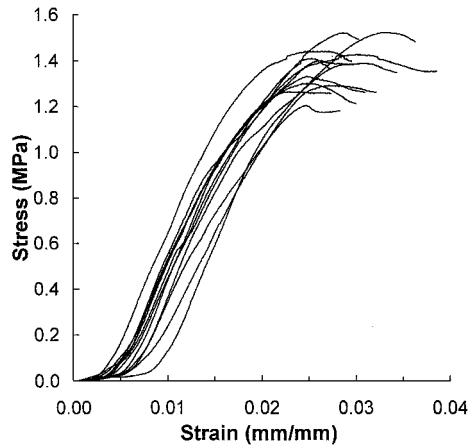


Fig. 7 Stress-strain curves obtained from parallel-compression testing of SIRCA 15A; density =  $311 \pm 9 \text{ kg/m}^3$ .

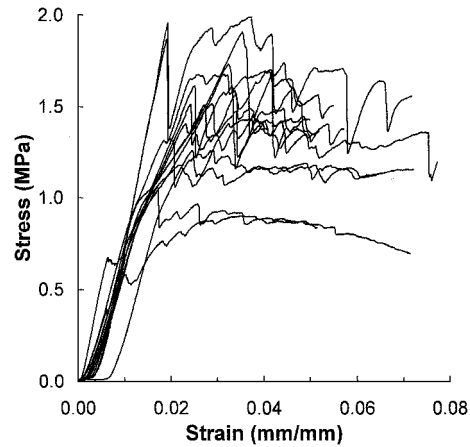


Fig. 10 Stress-strain curves obtained from parallel-compression testing of charred SIRCA 15A; density =  $243 \pm 8 \text{ kg/m}^3$ .

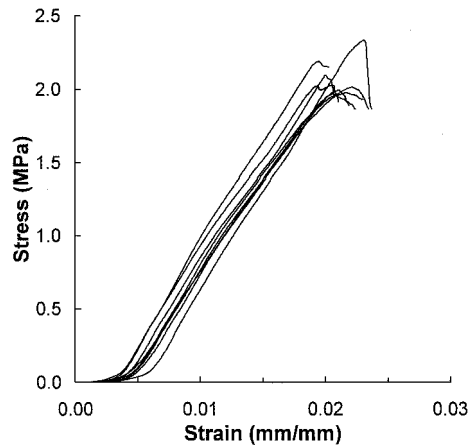


Fig. 8 Stress-strain curves obtained from parallel-compression testing of SIRCA 15F; density =  $260 \pm 4 \text{ kg/m}^3$ .

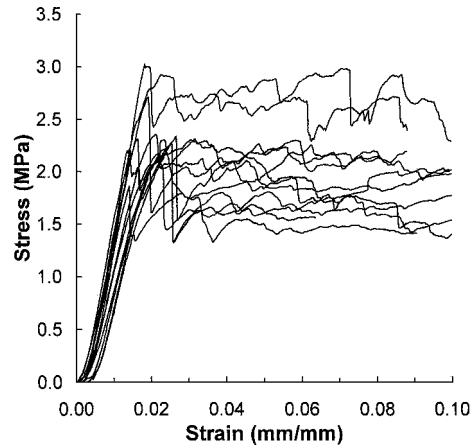


Fig. 11 Stress-strain curves obtained from parallel-compression testing of charred SIRCA 15F; density =  $253 \pm 21 \text{ kg/m}^3$ .

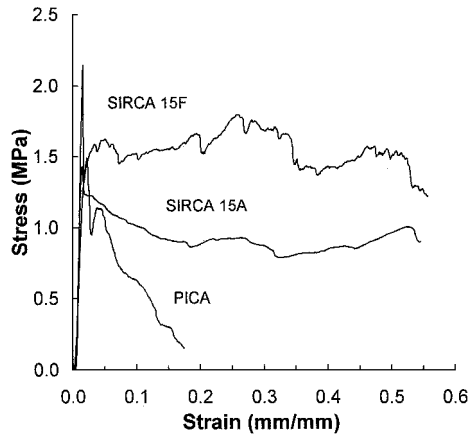


Fig. 9 Comparison of representative stress-strain curves of SIRCA 15A, SIRCA 15F, and PICA obtained from parallel-compression testing over a large range of strain.

stress-strain responses that are characteristic of a continuing, internal fracturing process. In parallel loading, the values of  $S$ ,  $E_1$ , and  $E_2$  of SIRCA 15F are about 50, 60, and 80% greater than the corresponding values for SIRCA 15A. Because FRCI is considerably stronger and stiffer than AIM, the relative strengthening and stiffening influences of the silicone resin are greater in SIRCA 15A than they are in SIRCA 15F. Specifically, in parallel loading, the compressive strength of SIRCA 15A is about three times that of AIM, whereas SIRCA 15F is about 70% stronger than FRCI. Likewise, the values of the secant moduli  $E_1$  and  $E_2$  of SIRCA 15A are about 70% greater than the corresponding values for AIM, whereas

the corresponding values of the secant moduli of SIRCA 15F and FRCI are comparable. Thus, for SIRCA 15F in parallel loading, the fibrous substrate is responsible for essentially all of the initial resistance to deformation.

The compressive responses of charred SIRCA 15A and charred SIRCA 15F are examined next because they had the same qualitative behavior (i.e., type 1) as the virgin LCAs under parallel loading and as the bare substrates under both modes of loading. Figures 10 and 11 show the parallel compressive responses of charred SIRCA 15A and charred SIRCA 15F specimens, respectively. The corresponding mechanical properties for the charred LCAs are listed in rows 7 and 8 of Table 1. Under parallel loading, the values of compressive strength and secant moduli of charred SIRCA 15A are comparable to the corresponding values for virgin SIRCA 15A, within the limits of statistical variations of material properties. This is also the case for charred SIRCA 15F and virgin SIRCA 15F. Thus, a comparison of the AIM and FRCI substrate data in rows 1 and 2 of Table 1 with the corresponding data for charred SIRCA 15A and charred SIRCA 15F in rows 7 and 8 shows that, even after the silicone resin is pyrolyzed, the char residue continues to strengthen both fibrous substrates and stiffen the AIM substrate. As was observed with PICA,<sup>1</sup> the process of charring also introduces greater nonuniformity among the SIRCA samples, as is seen from the relatively greater scatter in Figs. 10 and 11, compared with Figs. 3, 4, 7, and 8. Figures 12 and 13, respectively, show the stress-strain responses of charred SIRCA 15A and charred SIRCA 15F specimens under transverse compression. As Figs. 12 and 13 show, the charred specimens subjected to transverse loading also exhibited a relatively high degree of nonuniformity. Accordingly, the standard deviations listed for the mechanical properties of the charred samples in rows 6–10 of Table 1 tend to be particularly large, especially for the stress at initial fracture  $S_0$  and the compressive strength  $S$ . Under transverse

**Table 2** Transverse mechanical properties of SIRCA (derived from Figs. 14 and 15) and PICA (from Fig. 7 in Ref. 1)

| Material  | No. of specimens | Density, kg/m <sup>3</sup> | $E_i$ , MPa | $\sigma_Y$ , MPa | $\sigma_a$ , MPa  | $\sigma_b$ , MPa | $\varepsilon_c$ , mm/mm |
|-----------|------------------|----------------------------|-------------|------------------|-------------------|------------------|-------------------------|
| SIRCA 15A | 12               | 245 ± 11 <sup>a</sup>      | 15 ± 2      | 0.29 ± 0.04      | 0.22 <sup>b</sup> | 0.12             | 0.97                    |
| SIRCA 15F | 10               | 259 ± 7                    | 34 ± 5      | 0.72 ± 0.08      | 0.53              | 0.12             | 1.00                    |
| PICA      | 11               | 221 ± 2                    | 12 ± 2      | 0.27 ± 0.06      | -0.29             | 0.55             | 1.00                    |

<sup>a</sup>Numerical values following ± signs are standard deviations.

<sup>b</sup>Upwardly concave portions of the stress-strain curves are described by the function  $\sigma = \sigma_a + \sigma_b/(\varepsilon_c - \varepsilon)^2$ .

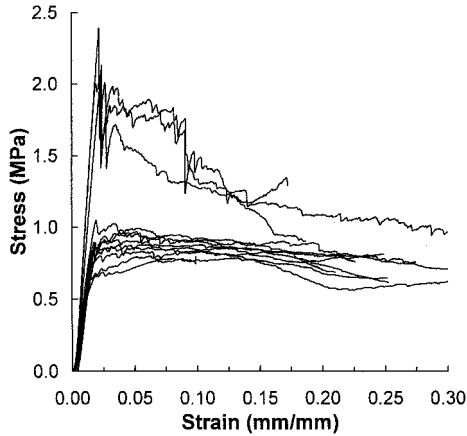


**Fig. 12** Stress-strain curves obtained from transverse-compression testing of charred SIRCA 15A; density = 268 ± 12 kg/m<sup>3</sup>.

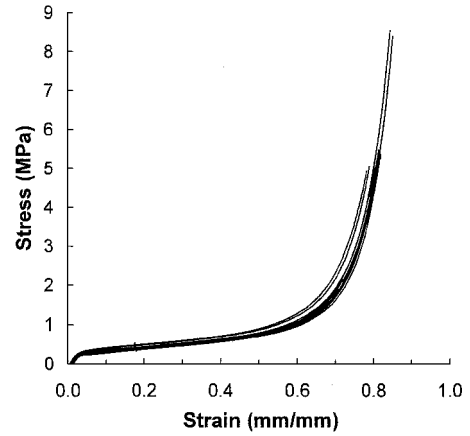


**Fig. 14** Stress-strain curves obtained from transverse-compression testing of SIRCA 15A; density = 245 ± 11 kg/m<sup>3</sup>.

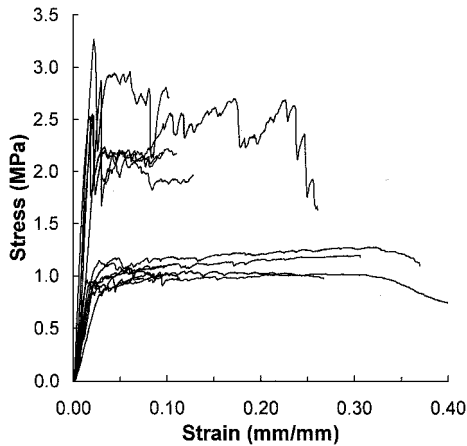


**Fig. 13** Stress-strain curves obtained from transverse-compression testing of charred SIRCA 15F; density = 244 ± 16 kg/m<sup>3</sup>.

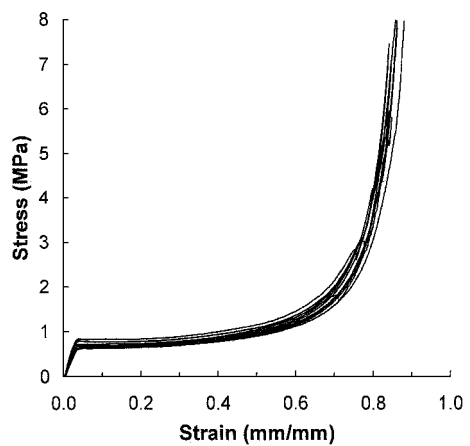


**Fig. 15** Stress-strain curves obtained from transverse-compression testing of SIRCA 15F; density = 259 ± 7 kg/m<sup>3</sup>.

load, charred SIRCA 15A is significantly stronger and stiffer than AIM, as is seen by comparing Figs. 5 and 12 and rows 3 and 9 in Table 1. In this mode, charred SIRCA 15F is also significantly stronger than FRCI, although the behavior of the charred samples varies widely; the weakest of the charred SIRCA 15F samples had compressive strengths that are comparable with the strongest FRCI samples, as is seen by comparing Figs. 6 and 13.

The most interesting influence of silicone impregnation was found in the transverse compression tests of virgin SIRCA 15A and virgin SIRCA 15F specimens; the stress-strain results from these tests are shown in Figs. 14 and 15, respectively. Here, the behavior is distinctly different from that found in the parallel testing of all specimens and in the transverse testing of AIM, FRCI, charred SIRCA 15A, and charred SIRCA 15F. The transverse compressive response for both types of SIRCA begins with a relatively linear increase in stress, up to strains of a few percent, after which the slope markedly decreases; the slope then begins to increase at an increasingly greater rate, up to strains over 80%. The stress-strain responses that exhibit these characteristics (regardless of whether fracture ultimately occurs) are designated as type 2. The transverse compression tests of PICA, charred PICA, and Fiberform also exhibited type 2 behavior,

although macroscopic fracture occurred at strains of about 60–70% (see Ref. 1). Some of the SIRCA 15F specimens did show evidence of internal fracture at strains in excess of about 50%, as seen from jogs in some of the stress-strain curves in Fig. 15, but these specimens still continued to support increasing stress with increasing strain; this increasing stress-strain phenomenon also occurred without observable barreling of the specimens.

Table 2 lists values of type 2 mechanical properties of the LCAs derived from the transverse compression tests of SIRCA 15A (Fig. 14), SIRCA 15F (Fig. 15), and PICA (Fig. 7 in Ref. 1). The method for determining the initial Young modulus  $E_i$  and initial yield stress  $\sigma_Y$  is described in Ref. 1. It is also shown here that the upwardly concave portions of the transverse stress-strain curves of the LCAs are described by the empirical equation

$$\sigma(\varepsilon) = \sigma_a + \sigma_b/(\varepsilon_c - \varepsilon)^2 \quad (2)$$

where  $\sigma_a$ ,  $\sigma_b$ , and  $\varepsilon_c$  are numerical parameters listed in Table 2. Figure 16 shows the analytic functions  $\sigma(\varepsilon)$  vs  $\varepsilon$  plotted together with experimental data points. Each datum point in Fig. 16 was calculated by averaging the measured stresses (in Figs. 14 and 15

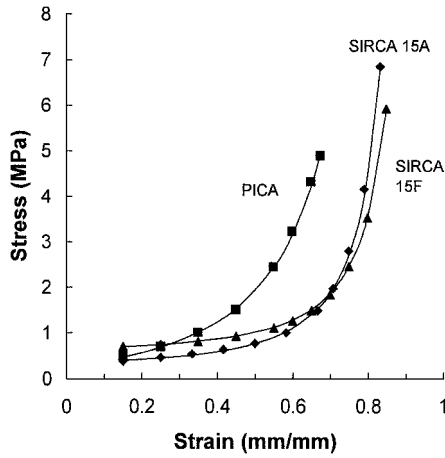


Fig. 16 Comparison of experimental stress-strain behavior (data points) with the empirical functions,  $\sigma = \sigma_a + \sigma_b/(\epsilon_c - \epsilon)^2$  (—), for SIRCA 15A, SIRCA 15F, and PICA in transverse compression.

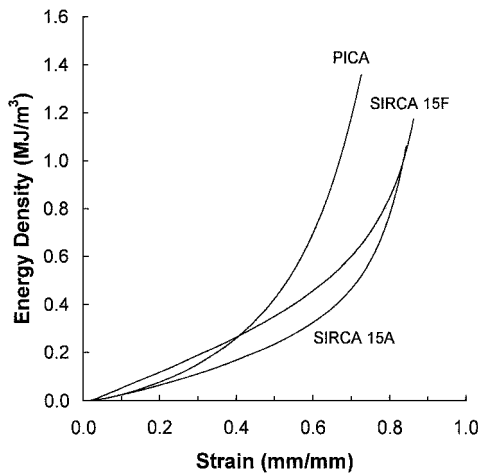


Fig. 17 Comparison of cumulative energy density vs strain for SIRCA 15A, SIRCA 15F, and PICA obtained from representative transverse-compression tests.

and in Fig. 7 of Ref. 1) at selected values of strain. The empirical parameters in  $\sigma(\epsilon)$  were fit to these data points in the following ranges of strain: 0.15–0.84 for SIRCA 15A, 0.15–0.85 for SIRCA 15F, and 0.15–0.68 for PICA. In each case, the critical strain  $\epsilon_c$  was found to be at, or very close to, unity, which indicates a theoretical asymptote at 100% strain. Figure 17 shows plots of energy density vs strain for representative transverse compression tests of SIRCA 15A, SIRCA 15F, and PICA. As Fig. 17 shows, under transverse compression, the LCAs are able to absorb considerable energy at large strains. Energy density  $e$  at strain  $\epsilon$  is the area under the stress-strain curve, given by

$$e(\epsilon) = \int_0^\epsilon \sigma(\eta) d\eta \quad (3)$$

Figures 18 and 19 show representative transverse stress-strain curves for each type of SIRCA, in its virgin and charred states, and for its corresponding substrate. The initial transverse responses of both types of SIRCA are somewhat similar to those of their corresponding substrates. For example, in the transverse mode, the initial yield stresses of SIRCA 15A and SIRCA 15F are  $0.29 \pm 0.04$  and  $0.72 \pm 0.08$  MPa, respectively (see Table 2), compared with stresses at initial fracture for AIM and FRCI of  $0.27 \pm 0.03$  and  $0.78 \pm 0.09$  MPa, respectively (see Table 1). However, after initial fracture, the substrates (as well as both charred SIRCA materials) exhibit continuing internal fracture, that is, the stress-strain pattern is roughly horizontal, with appreciable noise. Eventually, the substrates (and the charred SIRCA materials) cave in or collapse,

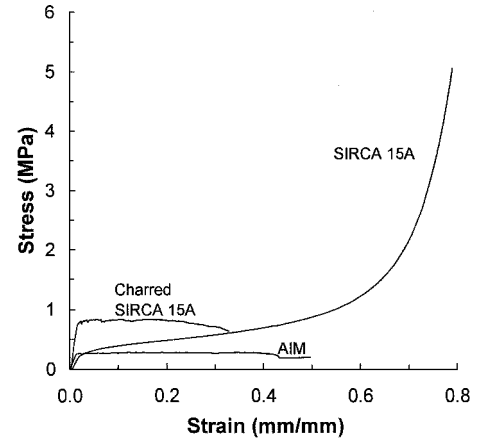


Fig. 18 Comparison of representative stress-strain curves of AIM, SIRCA 15A, and charred SIRCA 15A obtained from transverse-compression testing.

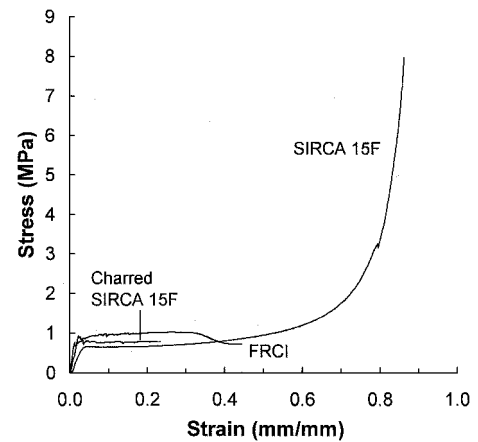


Fig. 19 Comparison of representative stress-strain curves of FRCI, SIRCA 15F, and charred SIRCA 15F obtained from transverse-compression testing.

whereas with increasing strain, the stress-strain curves of the LCAs continue to remain smooth, and they become concave upward. A significant difference between the SIRCA materials (and their substrates) and PICA (and its substrate) is that the latter (type 2) behavior was present in the transverse compressive responses of Fiberform and charred PICA, as well as in that of virgin PICA. This difference in behavior suggests that, in the transverse mode, at large strains, the fibers in Fiberform undergo relatively less fracture and/or debonding than do the fibers in AIM or FRCI.

#### Correlation of Hardness and Compressive Strength

Finally, the hardness  $H$  (see Table 3) and its correlation with compressive strength  $S$  are examined. In Ref. 1, for PICA, charred PICA, and Fiberform, wherein all parallel compressive responses were of type 1 and all transverse responses were of type 2, it is hypothesized that

... during parallel hardness testing, there exists highly localized separation and buckling in a small region beneath the indenter (since the dominant mechanism limiting compressive strength appears to be internal separation and buckling). As a result, the present method of measuring the hardness of LCAs may yield values that correlate well with compressive strengths in parallel loading. However, further testing with a wider variety of LCA materials needs to be carried out to establish any quantitative relationships.

As is discussed in the following paragraph, in the present study, good correlation was indeed found between compressive strength and hardness, not only for parallel loading tests, but for all tests resulting in type 1 behavior. In Ref. 1, it was also remarked that

**Table 3** Hardness of SIRCA, charred SIRCA, and the fibrous substrates AIM and FRCI<sup>a</sup>

| Material          | Density, kg/m <sup>3</sup> | Parallel loading |                    | Transverse loading |                    |
|-------------------|----------------------------|------------------|--------------------|--------------------|--------------------|
|                   |                            | No. of indents   | Hardness $H$ , MPa | No. of indents     | Hardness $H$ , MPa |
| SIRCA 15A         | 330                        | 7                | 2.45 ± 0.18        | 20                 | 1.66 ± 0.10        |
| AIM               | 170                        | 10               | 0.59 ± 0.05        | 5                  | 0.41 ± 0.01        |
| SIRCA 15F         | 240                        | 10               | 2.37 ± 0.43        | 20                 | 1.39 ± 0.10        |
| Charred SIRCA 15F | 256 ± 16                   | 10               | 3.55 ± 0.69        | 10                 | 2.06 ± 0.44        |
| Charred SIRCA 15F | 297 ± 36                   | 9                | 4.10 ± 0.92        | 10                 | 2.28 ± 0.40        |
| FRCI              | 220                        | 10               | 2.19 ± 0.32        | 5                  | 1.33 ± 0.09        |

<sup>a</sup>Numerical values following the  $\pm$  signs are standard deviations; where standard deviations are not listed for densities, a single value of density was determined for one bulk specimen.

**Table 4** Materials and test conditions associated with the data points (*a, b, ...*) in Fig. 20

| Datum point | Material <sup>a</sup> | Mode of loading | Density of $H$ samples, <sup>b</sup> kg/m <sup>3</sup> | Density of $S$ samples, <sup>c</sup> kg/m <sup>3</sup> |
|-------------|-----------------------|-----------------|--|--|
| <i>a</i>    | AIM                   | Transverse      | 170  | 165 ± 2  |
| <i>b</i>    | AIM                   | Parallel        | 170  | 192 ± 8  |
| <i>c</i>    | Fiberform             | Parallel        | 160  | 187 ± 6  |
| <i>d</i>    | FRCI                  | Transverse      | 220  | 182 ± 8  |
| <i>e</i>    | FRCI                  | Parallel        | 220  | 172 ± 5  |
| <i>f</i>    | SIRCA 15A             | Parallel        | 330  | 311 ± 9  |
| <i>g</i>    | SIRCA 15F             | Parallel        | 240  | 241 ± 1  |
| <i>h</i>    | SIRCA 15F             | Parallel        | 240  | 260 ± 4  |
| <i>i</i>    | Charred SIRCA 15F     | Transverse      | 256 ± 16   | 244 ± 16   |
| <i>j</i>    | Charred PICA          | Parallel        | 225 ± 2  | 225 ± 8  |
| <i>k</i>    | PICA                  | Parallel        | 220  | 220 ± 4  |
| <i>l</i>    | Charred SIRCA 15F     | Parallel        | 256 ± 16   | 253 ± 21   |

<sup>a</sup>Data for Fiberform, PICA, and charred PICA are from Ref. 1.

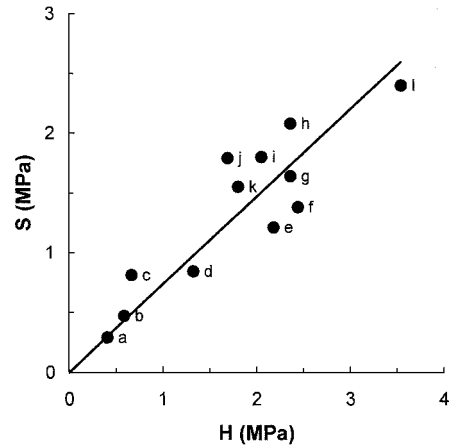
<sup>b</sup>Represents the average density of samples used to determine the average hardness  $H$  in each series of hardness tests.

<sup>c</sup>Represents the average density of samples used to determine the average compressive strength  $S$  in each series of compression tests.

... under transverse loading. ... the “representative stresses” exerted by the hardness indenter are in the non-linear, upwardly concave, regions of the stress-strain curves. ... Therefore, such stresses are too small to cause significant localized fracture, and in view of the complexity of the stress-strain curves, it may be presumed that hardness measurements are unlikely to correlate simply with compressive strengths.

This presumption, originally in reference to transverse testing of PICA, charred PICA, and Fiberform, apparently is applicable to cases associated with type 2 behavior, in general.

For those materials listed in Table 1 that exhibit type 1 behavior in both transverse and parallel compression, the ratios of transverse compressive strength to parallel compressive strength are in the range from about 0.6 (for AIM) to 0.8 (for charred SIRCA 15A). The ratio of transverse hardness to parallel hardness, for each material listed in Table 3, is in a comparable range (i.e., about 0.6–0.7), including even the virgin SIRCA materials (which can support transverse compressive stresses far in excess of their compressive strengths in parallel loading). Figure 20 is a plot of the average compressive strength vs average hardness for the materials that exhibit type 1 compressive behavior. The straight line has the form  $S = 0.73H$  and is the best least-squares, linear fit to the data, constrained to pass through the origin; the  $R^2$  value is 0.77. Table 4 identifies each datum point in Fig. 20 and lists the average densities of the specimens used in the determinations of the average values of  $S$  and  $H$  plotted in Fig. 20. Different samples were used for hardness and for strength measurements; variations in average density are owing to processing variables and/or material inhomogeneities. Some of the scatter in the data shown in Fig. 20 may be attributed to these density differences. For example, in cases where the average density of the hardness specimens is substantially greater than the average density of the compression test specimens (i.e., data points *d*, *e*, and *f*), it is expected that the data points would be skewed in the direction of higher hardness and, hence, would tend

**Fig. 20** Average compressive strength  $S$  vs average hardness  $H$  for LCAs, charred LCAs, and fibrous substrate materials that exhibited type 1 compressive behavior.

to lie below the least-squares line. Conversely, when the density of the compression test specimens is substantially greater than that of the hardness specimens (see data points *c* and *h*), the data points should lie above the least-squares line. These tendencies are indeed observed in Fig. 20. Also, the data for the charred specimens (*i*, *j*, and *l*) may be expected to deviate from the trendline because of the relatively large standard deviations of their average  $S$  and  $H$  values. In view of these considerations, there exists a good correlation between hardness and compressive strength over a wide range of samples that exhibit type 1 compressive behavior.

## Conclusions

This paper has presented results from compression and hardness tests on silicone impregnated reusable ceramic ablators (SIRCA) with the NASA designations SIRCA 15A and SIRCA 15F, in their virgin and charred states, and on their corresponding fibrous substrates, Ames insulation material (AIM) and fibrous refractory composite insulation (FRCI). AIM is made from silica fibers, and FRCI contains mainly silica and Nextel fibers. The materials have anisotropic mechanical properties because the fibers tend to align themselves parallel to a preferred plane. Therefore, two distinct modes of loading were employed, that is, load was applied parallel to the preferred plane of fiber alignment (referred to herein as parallel loading), and load was applied perpendicular to the preferred fiber-alignment plane (called transverse loading herein).

Two characteristic material responses, referred to herein as type 1 and type 2 behaviors, were observed during the compression tests. In type 1 behavior, the stress initially increased relatively linearly with strain, up to strains of about 1 or 2%, and then the stress followed an erratic, roughly horizontal, path as the strain increased. The erratic behavior in the latter stage indicates that bonds between the fibers, and/or the fibers themselves, were breaking in a discrete (i.e., discontinuous) manner as the material continued to deform. The substrates (AIM and FRCI), charred SIRCA 15A, and charred SIRCA 15F exhibited type 1 behavior under both parallel and transverse loading, and virgin SIRCA 15A and virgin SIRCA 15F exhibited type 1



behavior under parallel loading. Earlier parallel compression tests on phenolic impregnated carbon ablator (PICA), charred PICA, and Fiberform also resulted in type 1 behavior.<sup>1</sup>

The average compressive strengths of the materials that exhibited type 1 behavior ranged from 0.3 to 2.4 MPa. Specifically, under parallel compression, virgin SIRCA 15A had an average compressive strength of 1.4 MPa, and virgin SIRCA 15F had an average strength of 2.1 MPa. In parallel compression, SIRCA 15A was almost three times as strong as its bare substrate AIM, whereas SIRCA 15F was less than two times as strong as its bare substrate FRCI; however, FRCI is about two and a half times stronger than AIM in this mode. Therefore, the silicone impregnation had a greater relative influence on AIM than on FRCI. Also, under parallel compression, SIRCA 15F was about 50% stronger and 60–80% stiffer than SIRCA 15A. The materials that exhibited type 1 behavior in both modes of loading had ratios of strength in transverse compression to strength in parallel compression from about 0.6 to 0.7 (for the substrates) and about 0.8 (for the charred SIRCA materials). After pyrolysis, the char residue provided strengthening benefits to SIRCA 15A and 15F when compared to their corresponding substrates. However, greater error was associated with the numerical values of the mechanical properties of the charred materials owing to greater nonuniformities among the test specimens. For type 1 behavior, there was good correlation between hardness and compressive strength.

Virgin SIRCA 15A and 15F exhibited type 2 behavior under transverse loading. Earlier transverse compression tests for PICA, charred PICA, and Fiberform also resulted in type 2 behavior. In type 2 behavior, the stress initially also increased in a relatively linear manner with strain, up to strains of a few percent, and then the slope of the stress-strain curve decreased markedly. After this occurrence, the stress increased in an asymptotic manner wherein the stress varied with strain according to the empirical relation  $\sigma(\epsilon) = \sigma_a + \sigma_b/(\epsilon_c - \epsilon)^2$ , where  $\epsilon_c$  is a theoretical asymptote that is close to unity (i.e., 100% strain) and  $\sigma_a$  and  $\sigma_b$  are constants. Under transverse loading, both types of SIRCA supported stresses close to 10 MPa, at strains over 80%, without macroscopic fracture. Thus, the influence of silicone impregnation was most profound in the transverse mode of loading. The characteristic type 2 responses of SIRCA and PICA also enable the materials to absorb considerable energy under transverse compressive load. These responses may enable the materials to serve, not only for thermal protection of spacecraft, but also for absorbing impact during “hard” landings.

## Acknowledgments

This work was supported by NASA, Grants NAG 2-1148 and NCC 2-1049. The authors wish to thank Kirk Fields, the supervisor of the Materials Testing Laboratory at University of California Santa Barbara, for his help in implementing the experiments. The following student assistants are also acknowledged: Joe Mencher, Anthony DiCarlo, Edwin Guerra, Ryan Lotz, Patricia Valenzuela, and Christina Luna.

## References

- <sup>1</sup>Parmenter, K. E., Shuman, K., Milstein, F., Szalai, C. E., Tran, H. K., and Rasky, D. J., “Compressive Response of Lightweight Ceramic Ablators: Phenolic Impregnated Carbon Ablator,” *Journal of Spacecraft and Rockets*, Vol. 38, No. 2, 2001, pp. 231–236.
- <sup>2</sup>Tran, H. K., “Development of Lightweight Ceramic Ablators and Arc Jet Test Results,” NASA TM 108798, Jan. 1994.
- <sup>3</sup>Milos, F. S., and Squire, T. H., “Thermostructural Analysis of Silicone Impregnated Reusable Ceramic Ablator Tile for X-34 Wing Leading-Edge Thermal Protection System,” AIAA Paper 98-0883, Jan. 1998.
- <sup>4</sup>Tran, H. K., Johnson, C. E., Hsu, M.-T., Smith, M., Dill, H., and Chen-Jonsson, A., “Qualification of the Forebody Heatshield of the Stardust’s Sample Return Capsule,” AIAA Paper 97-2482, June 1997.
- <sup>5</sup>Tran, H. K., Johnson, C., Rasky, D., Hui, F., Chen, Y.-K., and Hsu, M., “Phenolic Impregnated Carbon Ablators (PICA) for Discovery Class Missions,” AIAA Paper 96-1911, June 1996.
- <sup>6</sup>Tran, H. K., Johnson, C., Rasky, D., Hui, F., and Hsu, M., “Silicone Impregnated Reusable Ceramic Ablators for Mars Follow-on Missions,” AIAA Paper 96-1819, June 1996.
- <sup>7</sup>Tran, H. K., Johnson, C. E., Rasky, D. J., Hui, F. C. L., Hsu, M.-T., Chen, T., Chen, Y. K., Paragas, D., and Kobayashi, L., “Phenolic Impregnated Carbon Ablators (PICA) as Thermal Protection Systems for Discovery Missions,” NASA TM 110440, April 1997.
- <sup>8</sup>Chen, Y.-K., and Milos, F. S., “Ablation and Thermal Response Program for Spacecraft Heatshield Analysis,” AIAA Paper 98-0273, Jan. 1998.
- <sup>9</sup>Marshall, J., and Cox, M. E., “Gas Permeability of Lightweight Ceramic Ablators,” *Journal of Thermophysics and Heat Transfer*, Vol. 13, No. 3, 1999, pp. 382–384.
- <sup>10</sup>Marshall, J., and Milos, F. S., “Gas Permeability of Rigid Fibrous Refractory Insulations,” *Journal of Thermophysics and Heat Transfer*, Vol. 12, No. 4, 1998, pp. 528–535.
- <sup>11</sup>Parmenter, K. E., and Milstein, F., “Mechanical Properties of Silica Aerogels,” *Journal of Non-Crystalline Solids*, Vol. 223, No. 1, 1998, pp. 179–189.

M. P. Nemeth  
Associate Editor